American Journal of Polymer Science 2015, 5(1A): 18-27
DOI: 10.5923/s.ajps.201501.03

Corrosion Resistant Polypyrrole/Flyash Composite Coatings Designed for Mild Steel Substrate

G. Ruhi*, H. Bhandari, S. K. Dhawan

Polymeric & Soft Materials Section, CSIR-National Physical Laboratory, New Delhi, India

Abstract Polypyrrole-flyash (PPy-flyash) composite was synthesized by chemical oxidative emulsion polymerization of pyrrole monomer using $FeCl_3$ as an oxidant. The synthesized composite was loaded in epoxy resin and subsequently coated on mild steel substrate using powder coating technique. XRD and FTIR analyses of the synthesized composite show the interaction between polypyrrole and flyash. SEM micrograph shows the embedded flyash particles in polypyrrole matrix. TGA thermograms show good thermal stability of the PPy-flyash composite as compared to neat polypyrrole. TGA thermograms of the coatings (epoxy alone and epoxy with different wt% loading of PPy-flyash composite) show appreciable increase in the thermal degradation temperatures of the coatings with PPy-flyash composite. Corrosion studies in 3.5% NaCl solution suggest significantly high corrosion protection efficiency (%P.E.) and high pore resistance (R_{pore}) for the epoxy coating with 2.0wt% loading of PPy-flyash composite (PF2). The EIS data obtained for the coatings exposed to 3.5% NaCl solution for 30 days show a superior corrosion resistance offered by the specimen PF2. The enhanced corrosion resistance of the coatings is due to the synergistic interaction between polypyrrole and flyash in the composite. Here, polypyrrole provides anodic protection to the steel substrate, whereas, flyash particles reinforce the integrity of the coating under corrosive conditions.

Keywords Coatings, Polypyrrole, Flyash, EIS

1. Introduction

Mild steel is a versatile engineering material because of its low cost, superior mechanical strength and good machinability. However, tendency to corrode limits its service life in various industrial applications. Application of corrosion resistant coatings can prevent or delay the degradation of steel exposed to aggressive environments, like sea water [1-4].

Flyash is a solid by product, generated in huge quantity during combustion of coal in thermal power stations. The mass scale dumping of flyash has led to severe environmental threat by contaminating surrounding air and land area. Therefore, utilization of flyash in various applications is required to avoid these problems [5-7]. Flyash, being rich in metal oxides like SiO_2, Al_2O_3, Fe_2O_3 and TiO_2, has tremendous potential in corrosion protection purposes. The ternary blends of flyash cement and silica fume is reported to improve the resistance to chloride ion penetration and reduce corrosion significantly [8]. Further, the fineness of fly ash improves the pore refinement and minimizes the access to deteriorating agents even at accelerated corrosion process [9]. Flyash as filler is important from both economic and commercial point of view [10-12].

Conjugated polymers like polypyrrole (PPy), polyaniline (PANI) have been identified as corrosion inhibitors. The oxidizing property of these polymers provides anodic protection to the metal surface. Polypyrrole is a well known conjugated polymer because of its environmental stability, biocompatibility, physical and electrical properties. It is reported as a suitable coating material for corrosion protection purpose [13-15]. However, mechanical integrity and thermal stability of these polymeric coatings in harsh climatic conditions are still questionable.

The objective of this work is to design polypyrrole-flyash (PPy-flyash) composite coatings for corrosion protection of mild steel substrate. The corrosion inhibition property of polypyrrole and reinforcing ability of flyash is utilized to design coatings with superior corrosion resistance for saline conditions. Electrochemical Impedance Spectroscopy (EIS) and Tafel plots were employed for the electrochemical characterizations of the test specimens. The coated specimens were exposed to Salt spray fog chamber to evaluate the corrosion resistance under accelerated test conditions.

2. Experimental Procedures

2.1. Chemicals and Materials

* Corresponding author:
drgazala24@yahoo.co.in (G. Ruhi)
Published online at http://journal.sapub.org/ajps

Pyrrole (Acros Organics) was distilled and stored under nitrogen at 4°C for further use. Sodium lauryl sulphate (SLS) and ferric chloride ($FeCl_3$) were purchased from Merck Chemicals. A fine cenosphere type flyash powder was collected from the Badarpur Thermal Power Plant, India. Iron oxide was removed using a magnetic bar. Froth floatation method was used to remove the carbon content and dust impurities. The chemical composition of cleaned flyash shows that it has SiO_2 (60–70%) and alumina (10–18%) as major constituents and MgO and alkalies varied between 1 and 5% each. The low carbon steel sheet of thickness 2 mm of composition, C = 0.18%, Mn = 0.5%, P = 0.04%, S = 0.06% and Fe = balance, is used as substrate. The steel specimens were obtained by cutting the steel sheet to a dimension of 10mm x 40mm x 2mm for corrosion studies and 150mm x 100 mm x 2mm for salt spray tests. The cut specimens were polished metallographically by grinding them with emery papers of 120, 600 and 800 grit size to attain a smooth finish. Thereafter, the steel specimens were degreased properly with acetone and kept in desiccator.

2.2. Synthesis of the Polymer Composite

Chemical oxidative polymerization of pyrrole monomer was carried out in presence of $FeCl_3$ to synthesize PPy-flyash composite. Flyash was added as filler by taking 10 wt% of pyrrole monomer. First of all flyash particles were dispersed in deionised water using a mechanical stirrer. 0.05 M of sodium lauryl sulphate (SLS) was added to the above suspension with continuous stirring. Afterwards, 0.1 M of pyrrole was added slowly followed by drop wise addition of ferric chloride solution (0.2M). The polymerization of pyrrole occurred with the appearance of black colour in the reaction suspension. The polymerization was carried out at room temperature for a period of 4-5 hrs. The obtained black suspension was filtered and washed thoroughly with ethanol and water. Thereafter, the synthesized black powder was dried under vacuum at 60°C.

2.3. Development of the Coatings

The synthesized polymer composite was blended with epoxy powder coating formulation in various wt% loadings (1.0, 2.0, 3.0 and 4.0%) using a laboratory ball mill. The composition of epoxy powder coating formulation is as follows: resin {epoxy (bisphenol A+polyester) (70%), Flow agent (D-88) (2.3%), degassing agent (benzoin) (0.7%), fillers (TiO_2 and $BaSO_4$) (27%). A homogeneously mixed polymer composite in epoxy was applied on mild steel specimens using an electrostatic spray gun held at 67.4 KV potential. The powder coated steel specimens were baked in oven at 180°C for 30 minutes. The epoxy coating developed on steel substrate is designated as EC and epoxy coatings with different wt% loading of polymer composite are designated as PF1 (1.0%), PF2 (2.0 %), PF3 (3.0%) and PF4 (4.0%).

2.4. Characterizations

2.4.1. Characterization of the Polymer Composites

Fourier Transform infrared (FTIR) spectroscopy (Model-Nicolet 5700) was employed in the spectral range of 4000-600cm^{-1} to analyse the chemical composition of the PPy-flyash composite. Scanning Electron Microscope (JEOL- JSM-6360A) was used estimate the size of the flyash particles and the morphology PPy-flyash composite. The energy dispersive X-Ray (EDX) was used to determine the elemental composition of the composite. X-Ray diffraction technique (Bruker D8 Advanced diffractometer) was employed to check the crystallinity of flyash and PPy-flyash composite. The thermal stability of the composite was analyzed using thermogravimetric analysis (TGA) (Mettler Toledo TGA/SDTA 851) at a heating rate of 15°C min^{-1} in nitrogen atmosphere.

2.4.2. Characterization of the Coatings

TGA of the final coating composition was carried out at a temperature range of 25°-700°C to evaluate the thermal stability of the designed coatings.

2.4.3. Electrochemical Characterization of the Coatings

Open Circuit Potential (OCP) vs time, Tafel polarization and Electrochemical Impedance Spectroscopy (EIS) was carried out using a traditional three electrode cell system Autolab Potentiostat/ Galvanostat, PGSTAT100 (NOVA Software). A three electrode cell assembly having coated steel specimens (1 cm^2 area exposed) were taken as working electrodes, Pt as counter electrode and Ag/AgCl as reference electrode. All the tests were conducted in 3.5% NaCl solution at room temperature (25±2ºC). The test specimens were allowed to attain equilibrium in NaCl solution under open circuit potential (OCP) condition, for 60 minutes prior to the electrochemical tests. Tafel plots were obtained by carrying out potentiodynamic polarization at a constant scan rate of 1mV/sec by sweeping the potential between ±100 mV vs Ag/AgCl from E_{corr}. The values of corrosion potential (E_{corr}), corrosion current density (i_{corr}), anodic (β_a) and cathodic (β_c) Tafel constants were extracted from Tafel plots. EIS was performed to extract the values of pore resistance (R_{pore}) and coating capacitance (C_c) by applying a sine potential signal of 10 mV in a frequency range of 100 KHz to 0.1 Hz at OCP. The values were derived by fitting suitable equivalent circuits. The corrosion protection efficiency (%P.E.) was determined from the measured i_{corr} {corrosion current density of uncoated steel ($i°_{corr}$) and corrosion current density of coated steel (i^c_{corr})} values by using the relationship [16] as mentioned in Equation 1.

$$\% \text{ P.E.} = (i°_{corr} - i^c_{corr})/i°_{corr} \times 100 \quad (1)$$

Salt spray tests were carried out as per ASTM B117 method to assess the corrosion tolerance of the composite

coatings under accelerated test conditions. For this, the coated steel panels were exposed to salt spray fog containing 5.0% NaCl for 150 days.

3. Results and Discussions

3.1. FTIR and XRD Spectra

Figure 1 shows the FTIR spectra of flyash and PPy-flyash. The spectrum for flyash exhibits a band at 1090 cm^{-1}, which corresponds to asymmetric stretching of Si-O or Al-O. A low intensity peak at 782 cm^{-1} is due to the presence of quartz (SiO_2) and a peak at 552 cm^{-1} is due to presence of mullite (Al_2O_3) in the flyash. The FTIR spectrum of PPy-flyash shows a peak at 1540 cm^{-1} corresponding to typical pyrrole ring vibration [17]. The low intensity peak at 1474 cm^{-1} is attributed to =CH in plane vibration. A peak of considerable intensity at 1038 cm^{-1} is the N–H in plane deformation absorption of polypyrrole. The corresponding peak of C-N stretching [18] of polypyrrole occurs at 1186 cm^{-1}which is shifted to 1166 cm^{-1} due to interaction between polypyrrole and flyash particles. The peaks at 782 cm^{-1} and 550 cm^{-1} shifted to 793 cm^{-1} and 561 cm^{-1}, respectively for PPy-flyash composite due to weak van der waal forces. The occurrence of a broad band in PPy-flyash composite at 3436 cm^{-1} is due to hydrogen bonding between N-H of polypyrrole and oxygen of SiO_2/Al_2O_3. The FTIR observations show synergistic interaction between polypyrrole and flyash particles.

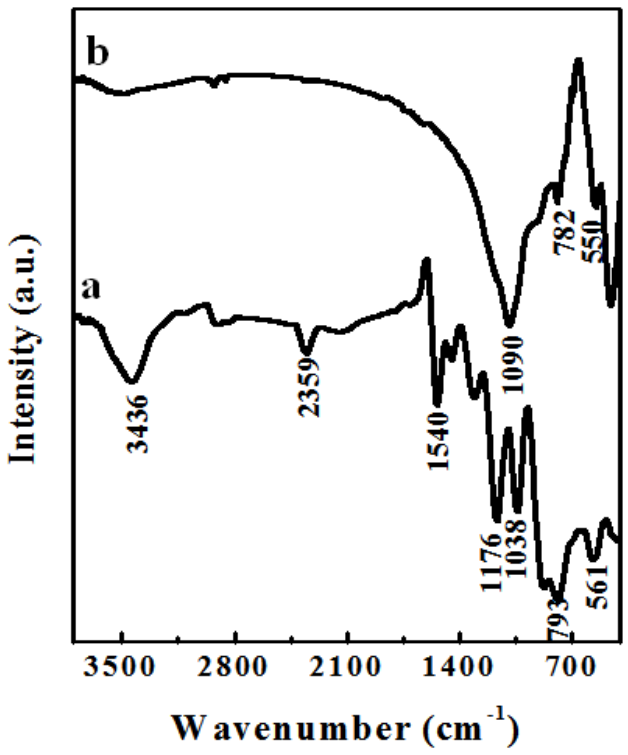

Figure 1. FTIR spectra of (a) Flyash and (b) PPy-flyash composite

The XRD plots of flyash and PPy-flyash are shown in Figure 2. The XRD plot for flyash shows well defined peaks of mullite (M) at a 2θ of 16.29° and 40.02°, quartz (Q) at 2θ of 20.86°, 26.58°, 35.13° and 49.96° and calcite (C) at 2θ of 33.4°. The presence of sharp peaks shows the crystalline nature of flyash, whereas, PPy-flyash composite exhibits a broad band at 2θ value of 25.7°. This reveals amorphous nature of the composite.

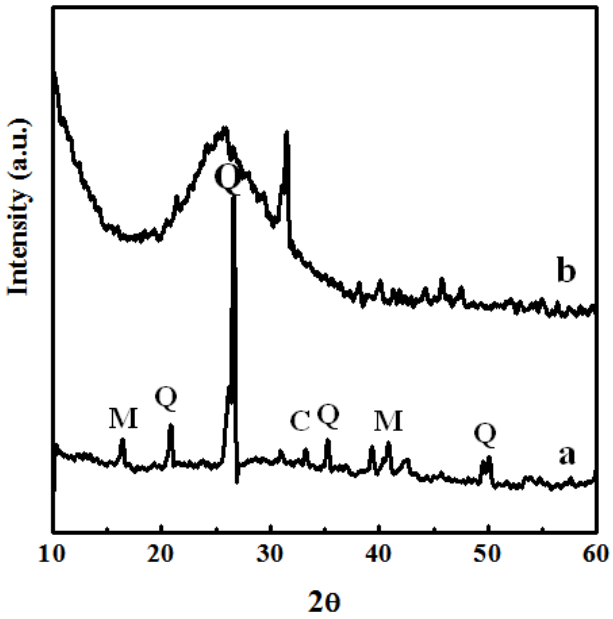

Figure 2. XRD spectrum of (a) flyash showing peaks of Mullite, Quartz and Calcite. The spectrum for (b) PPy-flyash composite shows its amorphous nature

3.2. Thermogravimetric Analysis (TGA)

The TGA thermograms of flyash, polypyrrole and PPy-flyash composite are shown in Figure 3. The thermograms were recorded by heating the samples at a temperature range of 25 to 700ºC under nitrogen atmosphere (60 ml/min). The flyash has shown high thermal stability with no weight loss over the entire range of temperature. The thermograms of polypyrrole and PPy-flyash indicated two stage weight loss. The first stage weight loss (5-6%) at 100º C is attributed to the loss of water molecules from the polymer matrix [19]. The second stage weight loss started at 234° and 285°C for polypyrrole and PPy-flyash, respectively. The corresponding weight loss represents the thermal degradation of polymer backbone [20]. Interestingly, a considerable enhancement of degradation temperature (50°C) is noticed for the PPy-flyash composite. This is basically due to the presence of flyash particles as filler in the polypyrrole matrix. Flyash is stable in the range from room temperature to 700°C and when incorporated in polypyrrole, restricts the thermal motion of the polypyrrole chains and shields the degradation of polymer [21]. The weight loss for polypyrrole and PPy-flyash composite at 700ºC is found to be 87% and 58%, respectively.

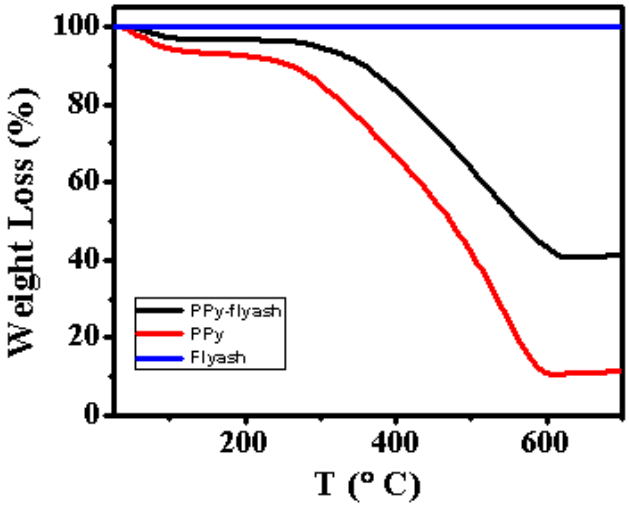

Figure 3. TGA thermograms of flyash, polypyrrole (PPy) and PPy-flyash

3.3. Microstructural Analysis

Figure 4a shows the SEM micrograph of flyash. The micrograph revealed the spherical morphology of flyash particles. The SEM micrograph of PPy-flyash composite (Figure 4b) showed a regular cauliflower like morphology of polypyrrole matrix embedded with flyash particles. The EDS analysis shows presence of elements, Carbon (62.1%), Oxygen (24.0%), Aluminium (1.4%), Silicon (2.5%) and Nitrogen (5.2%) in the composite.

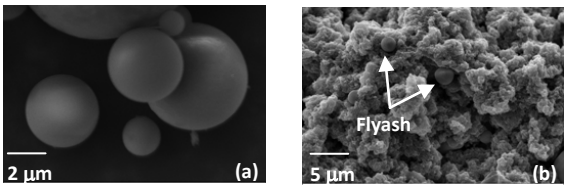

Figure 4. SEM micrograph of (a) flyash (b) PPy-flyash composite

3.4. TGA Thermograms of the Coating System

Figure 5 shows the TGA thermograms of coating formulations (epoxy and epoxy with different wt% loading of PPy-flyash composites). All the samples exhibited almost similar trends of weight loss. For epoxy, almost no weight loss is observed till the attainment of 347°C. However, an abrupt weight loss observed above this temperature shows the thermal degradation of epoxy resin. This is basically due to the physical cracking of the cross-linking of epoxy resin at this temperature. Interesting results are obtained for epoxy with 2.0, 3.0 and 4.0 wt% loading of PPy-flyash composite. An appreciable difference in the thermal degradation temperature of epoxy and epoxy with PPy-flyash composite is observed. The thermal degradation temperature of PF2, PF3 and PF4 occurred at 371°, 382° and 393°C, respectively. The appreciable shift of thermal degradation temperature clearly shows that the PPy-flyash composite enhances the thermal stability of epoxy resin.

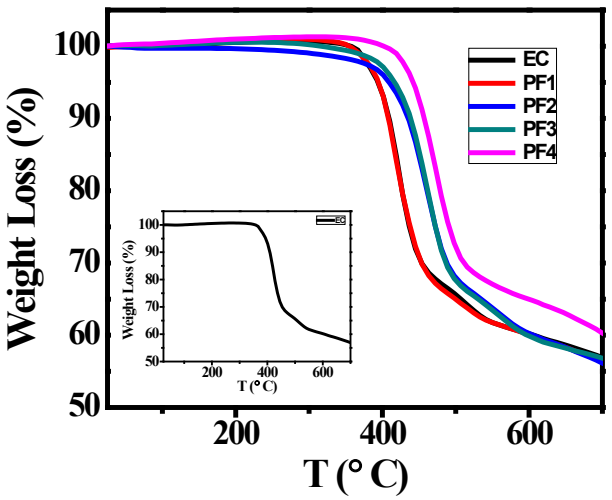

Figure 5. TGA thermograms of epoxy resin (EC) and epoxy with 1.0wt% (PF1), 2.0wt% (PF2), 3.0wt% (PF3) and 4.0wt% (PF4) loading of PPy-flyash

3.5. Corrosion Studies of the Coatings

3.5.1. Open Circuit Potential (OCP) vs Time

Figure 6 depicts the variation of OCP against time for epoxy coating (EC) and epoxy coatings with different wt% loading of PPy-flyash composite (PF1, PF2, PF3 and PF4) in 3.5% NaCl solution at room temperature (25±2°C). The trend of OCP variation for epoxy coating shows a sharp decrease of potential towards negative direction, within few minutes of immersion. This is due to the rapid diffusion of chloride ions through the coating. This was followed by the sudden shift of potential towards positive direction. However, the potential decreased steeply within few minutes and became almost stable till the end of the test. The steady state value of OCP for epoxy coating is observed to be 0.46 V vs Ag/AgCl. The epoxy coatings with PPy-flyash composite have demonstrated almost similar trend of the OCP variation with the passage of time. The OCP of the specimens PF1, PF2 and PF3 shifted negatively followed by a positive shift till the end of immersion time. The positive shift of OCP basically shows the passive state of under lying metal because of the good corrosion protection ability of the surface film [22]. However, trend of OCP variation of epoxy coating with 4.0% loading of PPy-flyash (PF4) shifted sharply towards negative potential after 76 minutes of immersion. This shows the rapid diffusion of chloride ions through the coating to the metal surface. The steady state values of OCP for specimens PF1, PF2 and PF3 is measured to be 360 mV, 280 mV and 350 mV more positive than the specimen EC. The occurrence of high positive OCP values is due to the effective barrier property of PPy-flyash composite towards the ingress of chloride ions to the metal surface.

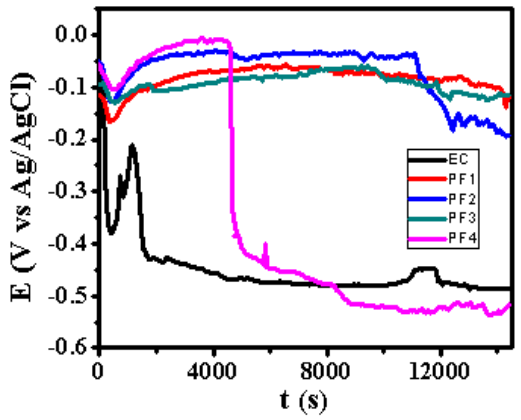

Figure 6. The OCP vs time graphs of epoxy coating (EC) and epoxy with 1.0wt% (PF1), 2.0wt% (PF2), 3.0wt% (PF3) and 4.0wt% (PF4) loading of PPy-flyash composite coatings in 3.5% naCl solution at 25±2°C

3.5.2. Tafel Plots

Figure 7 shows the Tafel polarization behaviour of epoxy coating (EC) and epoxy coatings with different wt% loading of PPy-flyash composite (PF1, PF2, PF3 and PF4) after 1 h of immersion in 3.5% NaCl solution at room temperature (25±2ºC). The plots were drawn to derive the values of different electrochemical parameters like corrosion current density (i_{corr}), anodic (β_a) and cathodic (β_c) Tafel constants by extrapolating the anodic and cathodic curve using Tafel extrapolation method (Table 1).

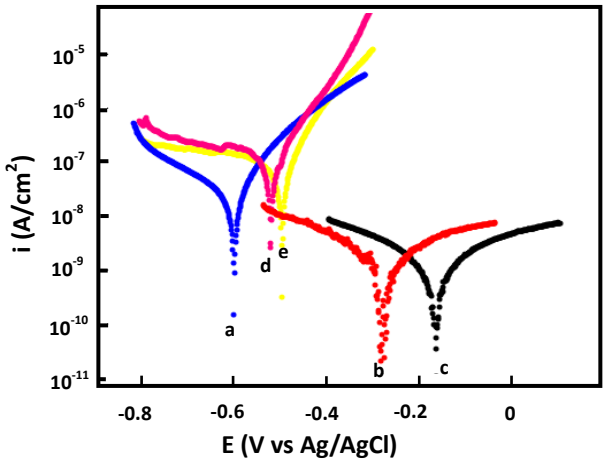

Figure 7. The Tafel plots of (a) epoxy coating and epoxy coatings with (b) 1.0wt% (PF1), (c) 2.0wt% (PF2), (d) 3.0wt% (PF3) and (e) 4.0wt% loading of PPy-flyash composite coatings in 3.5% naCl solution at 25±2°C

Table 1. Electrochemical Parameters Obtained from Tafel extrapolation in 3.5% NaCl solution

Sample Name	i_{corr} (A/cm^2)	β_a (mV/decade)	β_c (mV/decade)	(%P.E.)
EC	6.2×10^{-7}	359.5	96.1	----
PF1	6.4×10^{-9}	529.8	1247	98.9
PF2	5.8×10^{-9}	748.2	1038	99.0
PF3	1.3×10^{-7}	2078	92.4	79.1
PF4	1.4×10^{-7}	1924	111.4	77.4

From the measured data, it can be observed that the i_{corr} of epoxy coatings with 1.0% (PF1) and 2.0% (PF2) loading of PPy-flyash is two orders of magnitude and more than two orders of magnitude less, respectively as compared to epoxy coating (Table 1). Further, the occurrence of notably higher value of anodic and cathodic Tafel constants for specimens PF1 and PF2 implies the effective role of PPy-flyash composite in controlling anodic and cathodic corrosion reactions. The effective corrosion protection by PPy-flyash composite present as additive in the epoxy resin is the reason for the significant reduction in the values of i_{corr} for specimens PF1 and PF2. Accordingly, the corrosion protection efficiency (%P.E.) as calculated from equation 1 is observed to be 98.9 and 99.0% for specimens PF1 and PF2, respectively. The composite present in the epoxy resin acts as effective physical barrier against the penetration of chloride ions and protects the underlying metal surface. In addition to this, flyash particles provide mechanical integrity to the coating in 3.5% NaCl solution. In this way it behaves similar to other conventional coatings which restrict the penetration of ions through them. But the basic difference between conventional coatings and coatings with PPy-flyash composite is the polypyrrole, that provides anodic protection to the steel surface by shifting its potential to passive region [23-26]. This is due to the strong oxidative property of conjugated polymers that work as an oxidant to the steel surface (Figure 8). Here, PPy-flyash is added as an additive in the epoxy resin. However, the role of polypyrrole to intercept electrons at the metal surface and to transport them cannot be ruled out and it makes improvement in the corrosion resistance behaviour of the coatings [25]. Therefore, PPy-flyash composite delays the start of corrosion on mild steel surface. In this way it reinforces the corrosion resistance properties of the epoxy coating. However, the i_{corr} values increased with further loading of PPy-flyash composite in epoxy. The observed i_{corr} for specimens PF3 and PF4 is found to be almost five times higher as compared to epoxy coatings (EC) (Table 1). This could be due to the detrimental effect of the addition of PPy-flyash composite beyond 2.0wt% in epoxy system. It is speculated that 2.0wt% is the optimum limit of PPy-flyash loading in epoxy.

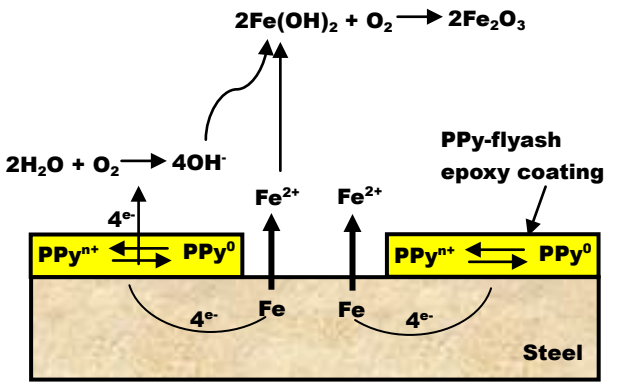

Figure 8. Schematic representation of corrosion resistance shown by PPy/flyash composite present in epoxy coatings

3.5.3. Electrochemical Impedance Spectroscopy (EIS)

Test specimens were kept at OCP conditions for 1 hr in 3.5% NaCl solution for impedance analysis. All the measurements were carried out at room temperature (25±2°C). The impedance graphs obtained for epoxy coating (EC) and epoxy coatings with different wt% loading of PPy-flyash composite (PF1, PF2, PF3 and PF4) are displayed in Nyquist plots (Figure 9) and Bode plots (Figure 11).

The Nyquist plot of specimen EC shows a small arc of semi-circle with a low value of impedance (Figure 9b). Interestingly, the Nyquist plot for specimen PF1 shows a high frequency capacitive behavisour followed by low frequency diffusion controlled behaviour of the coating. The capacitive behaviour shown by the specimen PF1 in the high frequency region demonstrates the corrosion resistance property of the coating, while the diffusion controlled behaviour in the low frequency region indicated the occurrence of diffusion process at the coating/metal interface [27]. The Nyquist plot for specimen PF2 shows capacitive and resistive behaviour with significantly high impedance. The corresponding Nyquist plots for specimens PF3 and PF4 exhibit a very small semicircle with a very low impedance value. The Nyquist plots of specimens EC, PF2, PF3 and PF4 have shown one time constant. Therefore, a simplistic circuit (Figure 10a) having a resistor connected in series to a parallel connected capacitor and resistor is applied to measure parameters like, pore resistance (R_{pore}) and coating capacitance (C_c). Whereas, for specimen PF1, (shows diffusion behaviour), an additional circuit element, Warburg impedance (W) is introduced in the equivalent circuit (Figure 10b).

The electrical resistance of a coating system is measured in terms of pore resistance (R_{pore}) and it signifies the performance of the surface coating. Whereas, coating capacitance (C_c) is an important parameter to measure the integrity of the coating and is related to water uptake tendency of the coating. Among the test specimens, the specimen EC evidenced the occurrence of a low pore resistance (R_{pore}) and high coating capacitance (C_c) (Table 2). This is due to the high water uptake by the epoxy coating due to its weak barrier property. The R_{pore} increased almost one and two orders of magnitude for specimen PF1 and PF2, respectively as compared to specimen EC. The specimen PF2 evidenced the highest R_{pore} ($1.2x10^7$ Ω) among the test specimens exhibiting its superior corrosion resistance property. The coating capacitance (C_c), occur in the decreasing order as, PF4, PF3, EC, PF1, PF2 (Table 2). The low coating capacitance observed for epoxy coatings with 1.0 and 2.0wt% loading of PPy-flyash composite is due to the low electrolyte uptake by the surface coating. However, the C_c increased with the further increase of the wt% loading of composite in the epoxy system. So, we can say that the increased wt% loading of PPy-flyash composite causes high electrolyte uptake and has a detrimental effect on the barrier property of the coating.

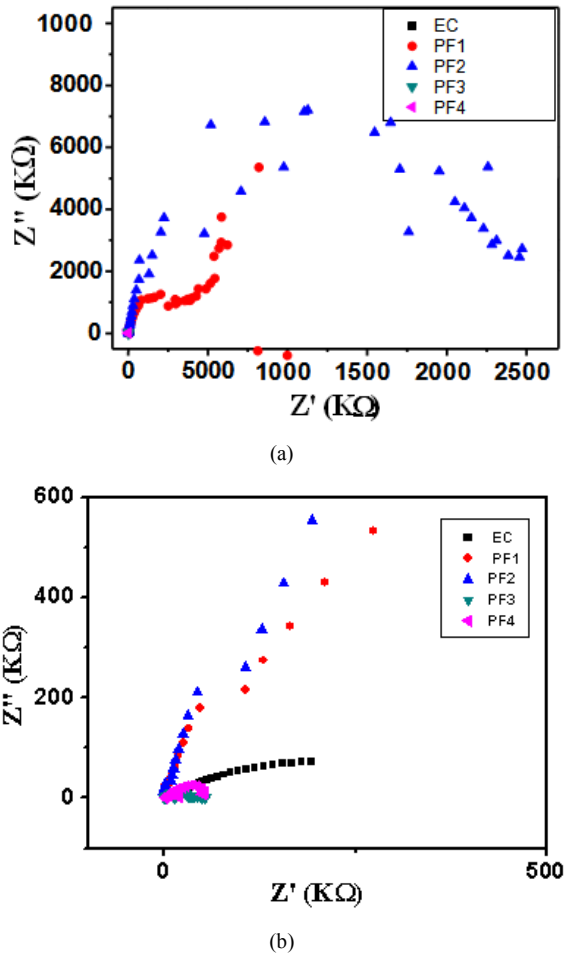

(a)

(b)

Figure 9. Nyquist plots of epoxy coating (EC) and epoxy coatings with 1.0wt% (PF1), 2.0wt% (PF2), 3.0wt% (PF3) and 4.0 wt% (PF4) loading of PPy-flyash composite in 3.5% NaCl solution at 25±2° C. A magnified view of high frequency region is shown in figure (b)

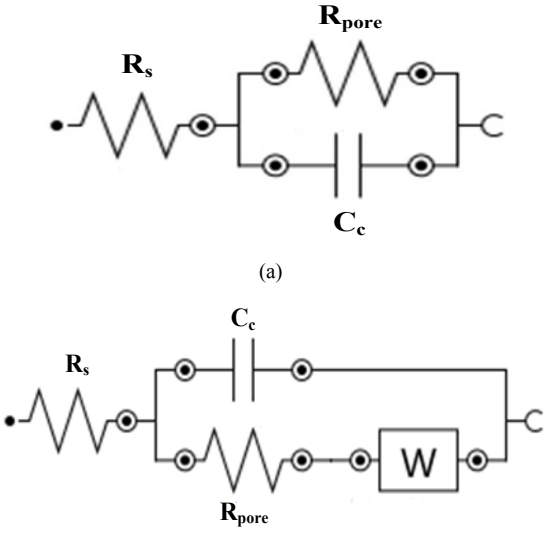

(a)

(b)

Figure 10. Electrical equivalent circuits of (a) intact coating in contact with 3.5% NaCl solution, (b) coatings showing diffusion of chloride ions. Here R_s is the electrolyte resistance, R_{pore} the pore resistance, C_c the coating capacitance

Table 2. Electrochemical Parameters Extracted by EIS Measurements in 3.5% NaCl solution

Sample Name	R_{pore} (KΩ cm^2)	C_c (nF/cm^2)
EC	56	1.71
PF1	2600	0.34
PF2	12000	0.28
PF3	30.3	3.33
PF4	32.7	3.61

The Bode plots, present the simultaneous measurement of modulus of impedance |Z| with respect to frequency, are shown in Figure 11 [28-30].

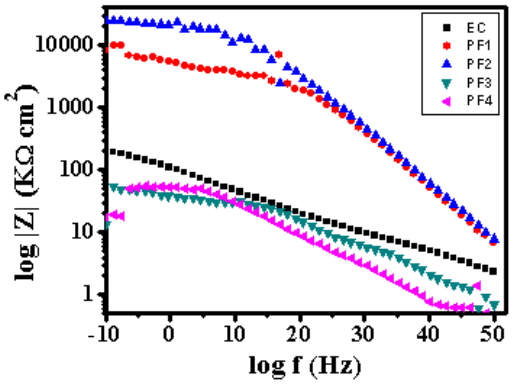

Figure 11. Bode plots of epoxy coating (EC) and epoxy coatings with 1.0wt% (PF1), 2.0wt% (PF2), 3.0wt% (PF3) and 4.0 wt% (PF4) loading of PPy-flyash composite in 3.5% NaCl solution at 25±2°C

The magnitude of impedance in low frequency region gives an idea about the barrier property of a surface film [31, 32]. The high magnitude of impedance in this region signifies high pore resistance towards the diffusion of electrolyte [32]. The Bode plots of specimens PF1 and PF2 show a straight line (slope -1) in the high frequency region. The slope of the plot becomes -1/2 in the lower frequency region with a high value of |Z| (Figure 11). The values of |Z| in this region, for specimens EC, PF3 and PF4 are observed to be low revealing the low pore resistance and easy electrolyte uptake tendency of the coatings. We can conclude that the epoxy coatings formed with 1.0 and 2.0wt% loading of PPy-flyash composite is compact in nature and has superior corrosion resistance in 3.5% NaCl solution. Epoxy coatings are well known for high adhesive strength due to the presence of polar groups in the structure which is chemically bonded to the steel surface. In the presence of corrosive environment, the interfacial bonding between epoxy/metal is destroyed because of the entry of electrolyte into the interface. This results in the failure of the coatings. Flyash particles act as a reinforcing material in the coating which enhances the mechanical integrity of the coating. It is presumed that the presence of flyash particles in coating matrix inhibit the penetration of electrolyte into the interface and enhance the corrosion protection efficiency.

The impedance data have shown that epoxy coatings with 1.0 and 2.0wt% loading of PPy-flyash have shown excellent corrosion resistance in the initial period of immersion (1 h) in 3.5% NaCl solution. However, evaluation of corrosion resistance of coatings for relatively longer period of immersion is equally important. Therefore, impedance parameters of the coatings are derived upto 30 days of immersion in 3.5% NaCl solution. The Nyquist plots of coatings started exhibiting two time constants after 24 h of immersion. The first time constant at higher frequency region corresponds to the capacitive behaviour of the coating whereas, the second time constant at low frequency region exhibits the diffusion controlled corrosion reaction occurring on the coating surface. Therefore, equivalent circuit as shown in Figure 10b (with Warburg impedance, W) is applied to derive the EIS parameters like R_{pore} and C_c. Figure 12 and 13 give the trend of the variation of R_{pore} and C_c, respectively with the passage of time. Figure 12 exhibits a high value of pore resistance (R_{pore}) for specimen PF2 even after 24 h of immersion. However, The R_{pore} reduced significantly up to 5 days of immersion. This trend was followed by a slow but gradual decrease of R_{pore} with immersion time. Specimens PF3, PF4 and EC exhibited very low R_{pore} values even during the initial period of immersion.

The values further decreased with the passage of time (Figure 12). The decrease of R_{pore} with time exhibits the weakening of the barrier property of the coating as the diffusion of electrolyte takes place through the coating. In accordance with the above results, the coating capacitance (C_c) is found to be low for the test specimens (Figure 13). However, it increased with the immersion time. The C_c is an important parameter that shows the water uptake tendency of a surface coating. Water has higher dielectric constant (ϵ = 80) and absorption of water by the coating results in the increase of the coating capacitance. So, it can be concluded that diffusion of electrolyte takes place through the coating resulting in the decrease of R_{pore} and subsequent increase of C_c. However, among the test specimens, The epoxy coating with 2.0wt% loading of PPy-flyash composite have shown highest R_{pore} and lowest C_c, exhibiting its superior corrosion resistance even during prolong immersion time.

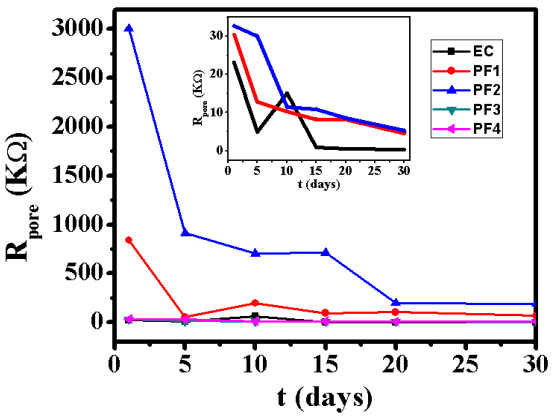

Figure 12. Variation of R_{pore} of epoxy coating (EC) and epoxy coatings with 1.0wt% (PF1), 2.0wt% (PF2), 3.0wt% (PF3) and 4.0 wt% (PF4) loading of PPy-flyash composite in 3.5% NaCl solution. The variation of R_{pore} of specimens EC, PF3 and PF4 is shown in inset

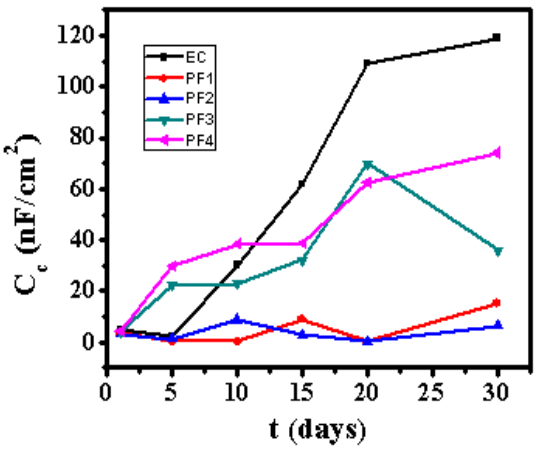

Figure 13. Variation of C_c of epoxy coating (EC) and epoxy coatings with 1.0wt% (PF1), 2.0wt% (PF2), 3.0wt% (PF3) and 4.0 wt% (PF4) loading of PPy-flyash composite in 3.5% NaCl solution

3.6. Salt Spray Test

Figure 14 shows the photographs of epoxy coated mild steel panels (EC) and epoxy with different wt% loading of PPy-flyash composite (PF1, PF2 and PF3) coated steel panels after exposure to salt spray fog for 150 days. Epoxy coated mild steel panel reveals the appearance of severe rusting and blistering along the scribe mark as shown in Figure 14a. The appearance of rust clearly indicates the loss of adherence of the epoxy coating to its substrate during prolong exposure to the salt spray fog. Several pin holes are also visible on the surface of epoxy coating.

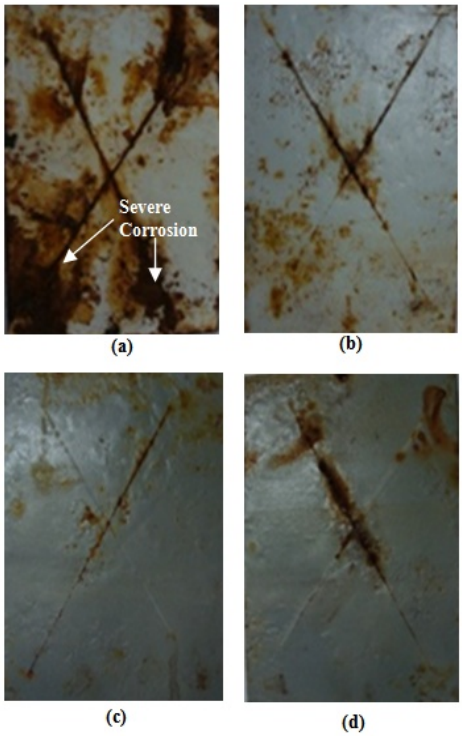

Figure 14. Photographs of (a) epoxy coated and epoxy with (b) 1.0wt%, (c) 2.0wt%, (d) 3.0wt% loading of PPy-flyash composite coated steel specimens exposed to salt spray fog after 150 days

This is due to the penetration of corrosive ions into the metal surface through the scribe mark. However, interesting results are obtained for epoxy with PPy-flyash composite coated panels. The PPy-flyash improves the corrosion resistance properties of the steel, as evident from the photographs (Figure14b, c and d). The specimen PF1 exhibited less extended corrosion along the scribe mark as compared to epoxy coated mild steel (Figure 14b). The situation further improves with 2.0 wt% loading of PPy-flyash in epoxy, as extension of corrosion is almost negligible along the scribe mark (Figure 14c). The observed results clearly show that the PPy-flyash composite provides effective corrosion protection for prolong period.The composite might have promoted the adhesion of the epoxy coating to the metal substrate improving its corrosion resistance under accelerated test conditions. However, as the loading of PPy-flyash increased beyond 2.0 wt%, spread of corrosion is evidenced along the scribe mark (Figure 14c). Therefore, 2.0wt% loading of PPy-flyash could be the threshold limit of the loading in epoxy system. The remarkably high corrosion protection offered by specimens PF1 and PF2 as compared to epoxy coating alone is due to the dual protection mechanism shown by the synthesized composite. Polypyrrole passivates the underlying metal and inhibits the diffusion of corrosive ions, whereas, flyash particles as reinforcing material, reduce the degradation of coating under corrosive conditions.

4. Conclusions

In this study, PPy-flyash composite was synthesized to design coatings for corrosion protection of mild steel substrate in 3.5% NaCl solution and under accelerated test conditions. The synergistic interaction between polypyrrole and flyash in the composite resulted in the improved thermal stability of the coatings. The corrosion resistant properties of the coatings were established from the results of Tafel polarization, impedance analysis and salt spray tests. In all these studies, epoxy coatings with 1.0 and 2.0 wt% loading of PPy-flyash composite exhibit significantly high corrosion resistance as compared to epoxy coating alone. The PPy-flyash composite acts as an effective barrier layer to passivate the metal surface and delay the degradation of coating under extremely corrosive conditions.

ACKNOWLEDGEMENTS

Authors thank the Director, (CSIR)-National Physical Laboratory, New Delhi for providing the laboratory facilities for conducting experiments and characterizations. Their thanks are extended to Mr. Brij Bisht for salt spray test results. One of the authors Gazala Ruhi is thankful to CSIR for her RA fellowship.

REFERENCES

[1] Rao, K. S., Sreedhar, N., Rao, B. M., Rao, K. P., 2004, Effect of pre-treatment on corrosion resistance of chromate conversion coated and anodized AA2219 Alloy, Transactions of Indian Institute of Metals, 57(2), 133-140.

[2] Chou, T. P., Chandrasekaran, C., Limmer, S., Nguyen, G., Cao, G. Z., 2002, Organic-inorganic sol-gel coating for corrosion protection of stainless steel, Journal of Material Science Letters, 21, 251–255.

[3] Guin, A. K., Nayak, S., Kumar, T., Bandhopadhyay, N., Kumar, D., 2011, Corrosion Resistance Nano-hybrid Sol-Gel Coating on Steel Sheet, ISIJ International, 51, 435-440.

[4] Caselis, J. L. V., Rosas, E. R., Meneses, V. M. C., 2012, Hybrid PMMA–silica anticorrosive coatings for stainless steel 316L, Corrosion Engineering, Science and Technology, 47(2), 131-137.

[5] Plowman, C., Shaw, N. B., 1984, Use of pulverizaed fuel ash as filler in plastics, Ash Tech, Conference Proceedings, London, England, pp 663-670.

[6] Jablonshi, G. J., 1987, Flyash Utilization as an extender in plastics and paints, Proceedings: Eighth International Ash Utilization Symposium, Palo Alto, CA, pp 38.1-38.15.

[7] Huang, X,. Huang, J. Y., Tieder, R., 1995, Clean fly ash as fillers in plastics, Proceedings; 11th International Symposium on use and Management of Coal Combustion by products (CCBS), 1, pp 33-1.

[8] Diab, A. M., Elyamamy, H. E., Elmonty, A. E. M. Abd., 2011, Effect of mix properties, sea water curing medium and applied voltages on corrosion resistance of concrete incorporating mineral admixtures, Alexandria Engineering Journal, 50(1), 65-78.

[9] Suntharajan, V. M., Sivakumar, A., 2013, Corrosion measurements in reinforced fly ash concrete containing steel fibres using strain gauge technique, International Journal of Corrosion, 2013, Article ID 724197- 7.

[10] Sathpathy, A., Sahu, S.P., Mishra, D., 2009, Development of protective coatings using flyash premixed with metal powder on aluminium substrates. Waste Management & Research, 9, 1-7.

[11] Kumar, B., Garg, R., Singh, U., 2012, Utilization of Flyash as filler in Hdpe/flyash polymer composite, International Journal of applied Engineering Research, 7(11), 1-4.

[12] Plaza, M. A. de la., Izquierdo, M. C., Bdabca, E. S. de la., Fuentes, I. H., 1999, Electro synthesis, electrochemical behaviour and structure of poly [bis(phenoxy phosphazene)]-polypyrrole doped composite film, Synthetic Metals, 106(2), 121-127.

[13] Xu, L., Chen, W., Mulchandani, A., 2005, Reversible conversion of conducting polymer films from superhydrophobic to superhydropholic, Angewandte Chemie, 44, 6009-6012.

[14] Schaftinghen, T. V., Deslouis, C., Hubin, A., Terryn, H., 2001, Influence of the surface pre-treatment prior to the film synthesis, on the corrosion protection of iron with polypyrrole films, Electrochimica Acta, 51, 1695-1703.

[15] Herrasti, P., Kulak, A.N., Bavykin, D.V., Ponce de Léon, C., Zekonyte, J., Walsh, F.C., 2011, Electrodeposition of polypyrrole–titanate nanotube composites coatings and their corrosion resistance, Electrochimica Acta, 56(3), 1323-1328.

[16] Sharifirad, M., Omrani, A., Rostami, A.A., Khoshroo, M., 2010, Electrodeposition and characterization of polypyrrole films on copper, Journal of Electroanalytical Chemistry, 645, 149-158.

[17] Radhakrishnan, S., Sonawane, N., Siju, C.R., 2009, Epoxy powder coating containing polyaniline for enhanced corrosion protection, Progress in Organic Coatings, 64, 383-386.

[18] Cheah, K., Forsyth, M., Truong, V.T., 1998, Ordering and stability in conducting polypyrrole, Synthetic Metals, 94, 215-219.

[19] Chandrakanthi, R.L.N., Careem, M.A., 2002, Preparation and characterization of CdS and Cu_2S nanoparticle/polyaniline composite films, Thin Solid Films, 417, 51-56.

[20] Bose, S., Kuila, T., Uddin, M.E., Kim, N.H., Lau, A.K.T., Lee, J.H., 2010, In-situ synthesis and characterization of electrically conductive polypyrrole/grapheme nano composites, Polymer, 51, 5921–5928.

[21] Zhang, W.H., Fan, X.D., Tian, W., Fan, W.W., 2012, Polystyrene/nano SiO_2 composite microspheres fabricated by pickering emulsion polymerization: Preparation, mechanisms and thermal studies, eXPRESS Polymer Letter, 6(7) 532–542.

[22] Mareci, D., Cailean, A., Ciurescu, G., Suliman, D., 2010, Electrochemical determination of the corrosion resistance of NiCr dental casting alloys, The Open Corrosion Journal, 3, 45-53.

[23] Iroh, J.O., Su, W., 2000, Corrosion performance of polypyrrole coating applied to low carbon steel by an electrochemical process, Electrochimica Acta, 46, 15-24.

[24] Wesseling, B., 1997, Scientific and commercial breakthrough for organic metals, Synthetic Metals, 85, 1313-1318.

[25] Sathiyanarayanan, S., Muthukrishnan, S., Venkatachari, G., 2006, Performance of polyaniline pigmented vinyl acrylic coating on steel in aqueous solutions, Progress in Organic Coatings, 55, 5-10.

[26] Nguyen, T.D., Nguyen, T.A., Pham, M.C., Piro, B., Normand, B., Takenouti, H., 2004, Mechanism for protection of iron corrosion by an intrinsically electronic conducting polymer, Journal of Electroanalytical Chemistry, 572, 225-234.

[27] Peebre, N., Picaud, T., Duprat, M., Dabosi, F., 1989, Evaluation of corrosion performance of coated steel by the impedance technique, Corrosion Science, 29, 1073-1086.

[28] Ruhi, G., Modi, O. P., Sinha, A.S.K., Singh, I.B., 2008, Effect of sintering temperatures on corrosion and wear properties of sol–gel alumina coatings on surface pre-treated mild steel Corrosion Science, 50, 639-649.

[29] Ruhi, G., Modi, O.P., Singh, I.B., 2009, Corrosion behaviour of nano structured sol-gel alumina coated 9Cr–1Mo ferritic steel in chloride bearing environments, Surface and Coatings Technology, 204, 359-365.

[30] Ruhi, G., Modi, O.P., Singh, I.B., 2009, Pitting of AISI 304L stainless steel coated with nano structured sol–gel alumina coatings in chloride containing acidic environments,

Corrosion Science, 5, 3057-3063.

[31] Metikos-Hukovic, M., Tkalcec, E., Kwokal, A., Piljac, J., 2003, An in vitro study of Ti and Ti-alloys coated with sol–gel derived hydroxyapatite coatings Surface and Coatings Technology, 165, 40-47.

[32] Belluci, F., Nicodemo, L., 1993, Water transport in organic coatings, Corrosion, 49, 235-247.